

## EFFECT OF FUEL DISTRIBUTION ON SPRAY DYNAMICS IN A TWO-STAGED MULTI-INJECTION BURNER

T. Providakis, L. Zimmer, P. Scouflaire, S. Ducruix

Ecole Centrale Paris - Laboratoire EM2C - CNRS  
Grande Voie des Vignes  
F-92295 Chatenay-Malabry  
France

Email: theodore.providakis@em2c.ecp.fr

### ABSTRACT

Burners operating in lean premixed prevaporized (LPP) regimes are considered as good candidates to reduce pollutant emissions from gas turbines. Lean combustion regimes result in lower burnt gas temperatures and therefore a reduction on the  $NO_x$  emissions, one of the main pollutant species. However, these burners usually show strong flame dynamics, making them prone to various stabilization problems (combustion instabilities, flashback, flame extinction). To face this issue, multi-injection staged combustion can be envisaged. Staging procedures enable fuel distribution control, while multipoint injections can lead to a fast and efficient mixing.

A laboratory-scale staged multipoint combustor is developed in the present study, in the framework of LPP combustion, with an injection device close to the industrial one. Using a staging procedure between the primary pilot stage and the secondary multipoint one, droplet and velocity field distributions can be varied in the spray that is formed at the entrance of the combustion chamber. Non-reactive and reactive flows are characterized through an extensive Phase Doppler Anemometry (PDA) campaign. Three staging values, corresponding to three different flame stabilization processes, are analyzed, while power is kept constant. It is shown that mean values and droplet distributions are affected by the staging procedure in the non-reactive as in the reactive situations. Using adequate post-processing, it is also possible to study non-reactive and reactive flow/flame dynamics. Spectral analysis shows that the non-reactive flow is strongly structured by a high frequency rotating structure that

can clearly be associated with a precessing vortex core (PVC), while the reactive situation encounters a strong acoustic-flame coupling leading to a low frequency oscillation of both the velocity field and the spray droplet distribution. In this last situation, high frequency phenomena, which may be due to PVC, are still visible.

### NOMENCLATURE

$D_{10}$	arithmetic diameter [ $\mu\text{m}$ ]
$D_{32}$	Sauter mean diameter [ $\mu\text{m}$ ]
$f$	frequency [Hz]
$\dot{m}$	mass flow rate [ $\text{g} \cdot \text{s}^{-1}$ ]
$\dot{Q}$	volumic flow rate [ $\text{l} \cdot \text{h}^{-1}$ ]
$P_w$	combustion power [kW]
$p$	acoustic pressure [Pa]
$q$	heat release rate [a.u.]
$St$	Stokes number [-]
$V$	velocity [ $\text{m} \cdot \text{s}^{-1}$ ]
$\alpha$	staging factor [%]
$\Delta P$	relative pressure [bar]
$\phi$	global equivalence ratio [-]
$\Phi$	Phase [-]
$\omega$	angular frequency [ $\text{rad} \cdot \text{s}^{-1}$ ]

### Subscripts

$()_a$	air
$()_{ac}$	acoustic
$()_{atm}$	atmospheric

- $()_f$  fuel
- $()_F$  flow
- $()_g$  global
- $()_p$  pilot stage
- $()_t$  takeoff stage
- $()_X$  axial
- $()_Z$  radial
- $()_\Phi$  phase

#### Superscripts

- $()'$  fluctuations
- $()^*$  re-sampled data
- $()^{NR}$  non-reactive
- $()^R$  reactive

## INTRODUCTION

Due to environmental concerns, permissible pollutant emissions of gas turbine plant or aircraft engines have been significantly decreased in recent years [1]. Combustion in gas turbines was traditionally based on non-premixed flames for various reasons (safety, stability), but this type of combustion leads to large pollutant emissions ( $\text{NO}_x$ , CO, ...). To face this issue, Lean Premixed Prevaporized (LPP) regimes are envisaged in new generation combustors [2, 3, 4]. This concept consists in providing a uniform lean mixture of fuel and air that burns at lower temperature than non-premixed flames, mainly reducing thermal  $\text{NO}_x$  emissions. Unfortunately gas turbines operating in lean conditions often present high combustion dynamics, leading to stability issues such as combustion instabilities, flashback, self-ignition and blowout [5]. In particular, the coupling of heat release and pressure oscillations in the combustor can produce self-excited oscillations of such an amplitude that they may damage the combustor [6, 7, 8]. It is known that these acoustic interactions tend to develop more easily in partially and perfectly premixed combustion systems such as the LPP ones [9]. As an example of what can be envisaged to overcome those problems, secondary fuel injection has been proposed, for which a small amount of fuel is injected upstream to constitute a piloting region. This secondary injection can also be modulated so as to reduce coupling between heat release and pressure while keeping reduced  $\text{NO}_x$  emissions [10, 11, 12, 13, 14].

Multi-injection staged injectors are now considered as potential candidates for real engine operations. Staging procedures enable fuel distribution control, while multipoint injections can lead to a fast and efficient mixing [15]. However, the dynamics of these new generation injection devices must still be studied to clearly determine their stability properties and to optimize spatial fuel distribution. In a recent work, a laboratory-scale multi-injection staged system was developed for gaseous fuel [16]. It was shown that the staging factor had a strong impact on flow dynamics, flame structure, combustion

instabilities.

The present paper concerns the study of a similar multi-injection system, fed with liquid fuel (dodecane) to be more representative of practical applications. Introducing a two-phase flow adds new complex parameters such as droplet distribution and evaporation that strongly influence the combustion dynamics. Depending on the type of atomizer used for fuel injection, strong fluctuations can be encountered in the resulting spray [17]. In the present study, a laboratory-scale staged multipoint combustor is developed in the framework of LPP combustion. Depending on the regime and staging factor, strong combustion instabilities can be encountered. Using the staging procedure between the primary and the secondary stages defined in [16], droplet and velocity field distributions can be varied in the spray that is formed at the entrance of the combustion chamber. Non-reactive and reactive flows are characterized through an extensive Phase Doppler Anemometry (PDA) campaign. Three staging values, corresponding to three different flame stabilization processes, are analyzed, while power is kept constant. Non-reactive and reactive flow, spray and flame dynamics are determined using spectral post-processing. A synchronized phase-lock averaging procedure is finally proposed to go deeper in the analysis of this highly coupled dynamics.

## EXPERIMENTAL SETUP

The multipoint staged is composed of two stages where air and liquid fuel can flow and mix. The resulting mixture enters a rectangular combustion chamber ( $500 \times 150 \times 150\text{mm}$ ), composed of two silica windows for optical access and two water-cooled walls.

### Injection device

A schematic view of the injection device is shown in Fig. 1. Inside the injection device, the upstream (primary) stage is called the 'Pilot stage'. It is composed of a pressurized nozzle for fuel distribution and a swirler for air injection. The pressurized nozzle generates a solid cone and fuel can be injected at a maximum flow rate of 6.3 liters per hour. Its flow number is equal to  $1.4 \text{ l} \cdot \text{h}^{-1} \cdot \text{bar}^{-0.5}$ . The air swirler is composed of 18 vanes and it is geometrically designed so that 20% of the global air rate flows through this stage. This has been checked experimentally in [16]. The downstream (secondary) stage is called the 'Takeoff stage'. It is composed of a multipoint system for the fuel and a swirler for the air. The multi-injection system is composed of 10 equally-spaced holes (0.3 mm in diameter). The swirler is composed of 20 vanes and it has been designed so that 80% of the global air rate flows through this stage. Both swirlers are set co-rotating (but this could be easily modified) and designed so that the swirl number  $S$  based on geometrical

**TABLE 1.** OPERATING AND PRESSURE CONDITIONS FOR BOTH NON-REACTIVE AND REACTIVE CONDITIONS.

$P_w = 85 \text{ kW}$ ,  $\phi = 0.6$ ,  $P_a = P_{atm}$ .

Condition	$\dot{m}_a [\text{g} \cdot \text{s}^{-1}]$	$\dot{Q}_{f,g} [\text{l} \cdot \text{h}^{-1}]$	$\alpha [\%]$
OP <sub>20</sub>	50	9.4	<b>20</b>
OP <sub>35</sub>	50	9.4	<b>35</b>
OP <sub>60</sub>	50	9.4	<b>60</b>

Condition	$\Delta P_{f,t} [\text{bar}]$	$\Delta P_{f,p} [\text{bar}]$	$\Delta P_a/P_a [\%]$
OP <sub>20</sub>	0.13	1.9	3 - 4
OP <sub>35</sub>	0.11	6	3 - 4
OP <sub>60</sub>	0.08	18	3 - 4

considerations is close to 1 [18]. To enhance spray vaporization, air is preheated at 473 K.

As staging is one of the main features of this type of injection system, a staging factor  $\alpha$  is defined to quantify the relative amount of fuel injected through the primary (pilot) injector [16]:

$$\alpha = \frac{\dot{m}_{f,p}}{\dot{m}_{f,g}} \times 100 \quad (1)$$

where  $\dot{m}_{f,g}$  is the total fuel flow rate and  $\dot{m}_{f,p}$  is the fuel flow rate through the primary stage. As a consequence,  $\alpha$  will be zero in case all fuel flows through the secondary (take-off) stage and 100% for all fuel injected through the pilot stage.

Table 1 shows the operating conditions chosen for the present study. The global air and fuel flow rates are kept constant (constant power and global equivalence ratio) while  $\alpha$  is varied from 15 to 60%, a domain where the shape of the flame is highly influenced by the stage procedure. For values of  $\alpha$  higher than 50% (pilot stage regimes), the flame stabilization process is controlled by the pilot stage, leading to a compact V-flame, anchored inside the injection device. For values of  $\alpha$  lower than 25% (take-off stage regimes), the flame is stabilized thanks to the take-off stage and takes an M-shape. In-between, there seems to be a competition between both stages, leading to a tulip-like shape of the flame. In the present study, measurements focus on three values of the staging factor (20, 35 and 60%), representative of the three flame shapes. It must be noticed that combustion instabilities are encountered in all cases, associated with a more or less strong acoustic activity depending on the staging, as described in Table 2.

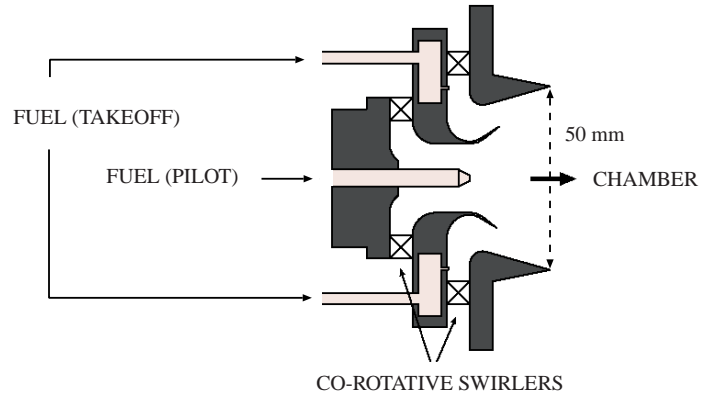


**FIGURE 1.** SCHEMATIC VIEW OF THE INJECTION DEVICE. FLOW FROM LEFT TO RIGHT.

**TABLE 2.** STABILIZATION MECHANISMS, THERMO-ACOUSTIC INSTABILITY FREQUENCIES  $f_{ac}$  AND AMPLITUDES  $p_{M2}$  FOR THE THREE OPERATING CONDITIONS.

Condition	Stabilization	$f_{ac} \text{ (Hz)}$	$p_{M2} \text{ (dB)}$
OP <sub>20</sub>	M-shape	300	133
OP <sub>35</sub>	Tulip-like shape	252	108
OP <sub>60</sub>	V-shape	280	133

## Diagnostics

**Spray characterization** The spray is characterized in both non-reactive and reactive conditions using the Phase Doppler Anemometry (PDA) technique. A Dantec dual-beam PDA system is installed in the present configuration allowing to measure the local distributions of droplet diameters and two velocity components. The system is composed of a 5 W Ar<sup>+</sup> laser with two lines respectively at 514 nm and 488 nm combined with a 40 MHz Bragg cell for frequency shift. Two lenses are used for the transmitting and receiving optics with respective focal lengths at 250 mm and 300 mm. The receiver is placed at 30° from the transmitter axis. A schematic view of the setup is shown in Fig. 2.

Data are acquired at different locations using an automatic two-axis translation system allowing high precision on the measurement location. Laser beam intersections are kept at the center of the chamber along the  $Y$  axis position, while location is varied on the  $X$  and  $Z$  axis. In the present study, only the results at  $X = 15 \text{ mm}$  will be discussed, as they are quite representative of what is observed elsewhere. A more exhaustive study will be proposed in the future.

Data rates between 0.2 (reactive) and 20 kHz (non-reactive situ-

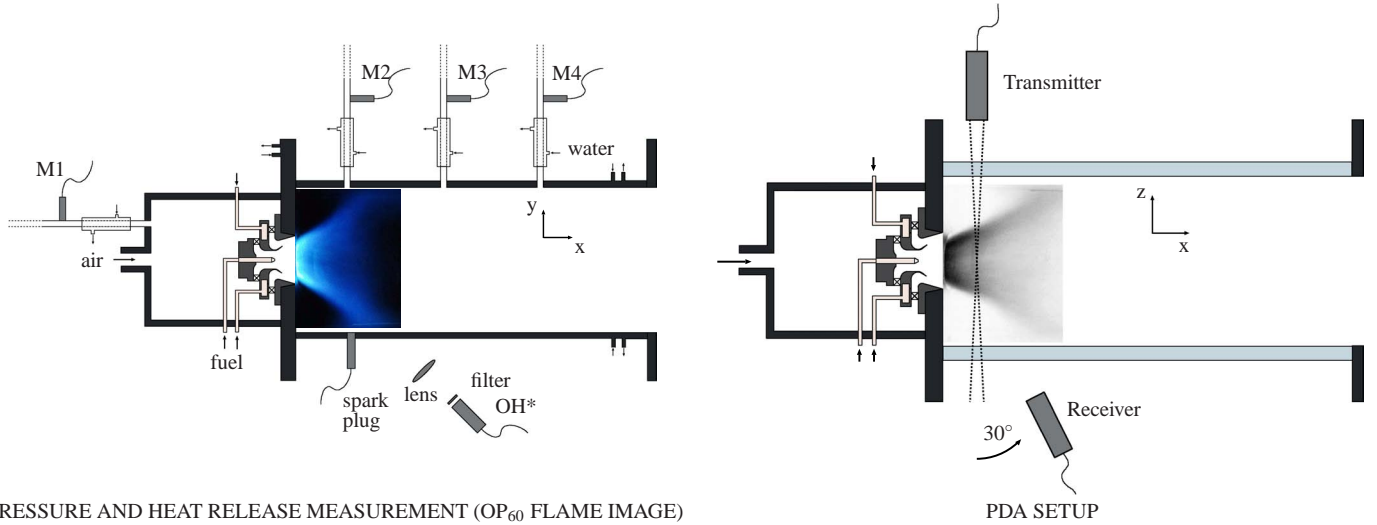


FIGURE 2. EXPERIMENTAL SETUP.

ations) and a minimum burst efficiency of 0.6 could be achieved. During tests, more than 100,000 samples are validated in the main regions of interest, whereas in low signal regions, the acquisition time is limited to 30 seconds, resulting on lower data rates.

**Pressure fluctuations and OH\* chemiluminescence** Four Bruel & Kjaer microphones (M1, M2, M3 and M4) are placed in semi-infinite water cooled waveguides that are flush-mounted close to the injection device and on the combustion chamber axis to measure pressure fluctuations (Fig.2). A Hamamatsu photomultiplier, coupled with a filter ( $\lambda = 310 \pm 10\text{nm}$ ) and a spherical lens (focal = 300 mm) to collect all the light emitted by the flame, is used to measure OH\* chemiluminescence. This last signal is supposed to be proportional to the heat release rate, giving access to heat release fluctuations, a crucial quantity in the understanding of combustion instabilities.

All signals are acquired simultaneously on a multi-port National Instruments acquisition card, at a rate of 16 kHz during 30 seconds, giving almost 500,000 samples per acquisition. In addition, pressure signal from microphone M2 and spontaneous emission from OH\* are also acquired simultaneously with the PDA ones, to enhance the time-signal reconstruction technique, which will be discussed in the results section.

## DATA PROCESSING

PDA softwares offer different techniques for acquisition validation. In the present study, a validation criterion was applied

to the diameter measurements. For each droplet, two independent size measurements allow to control the difference between the two values. In the present study, a difference larger than 10% leads to the droplet rejection. In addition to the validation criterion, both diameter and velocity signals are corrected by applying the transit time of a particle,  $\tau_i$ , as a weight factor. It is shown in [19,20] that this weight factor is well adapted for both velocities and diameters.

In order to perform spectral analysis methods, a re-sampling technique must be applied to the randomly sampled signals acquired with the PDA system. In this work, two sampling techniques have been tested on the signals.

(1) *The sample and hold technique* is the most classical one. In a few words, it consists in keeping the same physical value coming from the signal measured by the PDA until a new one is acquired. This can be expressed as:

$$t^* - t_{pda} \geq 0 \implies X^*(t^*) = X_{pda}(t_{pda}) \quad (2)$$

where  $t^*$  and  $t_{pda}$  are respectively the re-sampled and PDA times and  $X^*$  and  $X_{pda}$  are respectively the re-sampled and PDA values.

(2) *The sample and hold modified technique* consists in taking the physical value from the measured signal at the closest measured time. This can be written as:

$$|t^* - t_{pda}| = \min(|t^* - t_{pda}|) \implies X^*(t^*) = X_{pda}(t_{pda}) \quad (3)$$

In regions where high data rates were achieved, a re-sampling frequency of 16 kHz, for the non-reactive situation, and 6 kHz,

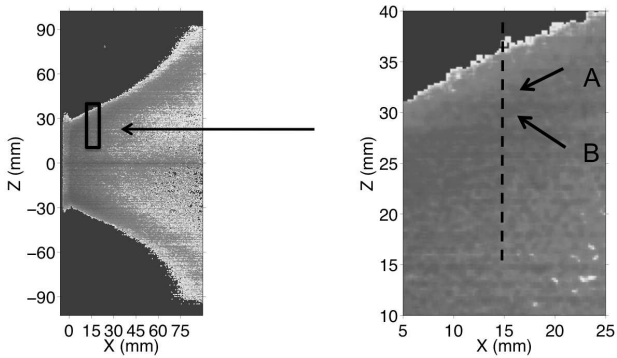


**FIGURE 3.** ABEL TRANSFORM OF THE TIME-AVERAGED OH\* CHEMILUMINESCENCE FOR OP<sub>60</sub> (LEFT). MEAN PROFILES ARE COMPUTED ALONG THE DOTTED LINE IN THE ENLARGEMENT (RIGHT). REGIONS A AND B CORRESPOND TO THE LOCATIONS OF SPECTRAL ANALYSIS.

for the reactive one could be used with both techniques. It was shown that both lead to very similar spectral contents, and the main frequencies could be properly retrieved. To discriminate between both techniques, several tests were carried out. They show that the hold sample technique leads to an average percentage of constant consecutive values of about 25%, while this percentage is only 15% when using the modified one. In the present study, only the results using the modified technique are presented.

## RESULTS AND DISCUSSION

Profiles of the mean flow are first presented at  $X = 15$  mm,  $Y = 0$  mm and  $Z$  between 15 and 40 mm for one side of the flow only, as shown on Fig. 3. No results will be presented closer to the axis of symmetry of the burner, since few or no droplets were encountered.

### Axial and radial mean velocities

Figures 4(a), 4(b), 5(a) and 5(b) show the mean profiles of the radial and axial velocities for non-reactive and reactive cases. The global shape of the profiles is the result of the inner and outer recirculation zones (IRZ and ORZ) usually expected in highly swirling flows [21]. These two zones tend to confine the droplets in the conical penetration region of the fresh gases, where higher axial velocities are reached. In addition, results indicate a global increase of both velocities in reactive conditions due to the high temperature of the flow

In the non-reactive situations, little influence of  $\alpha$  is observed on the velocity fields. High axial velocities and radial velocities close to 0 are visible in the heart of the spray. In addition, the radial velocity  $\bar{V}_z$  profile shows negative values in the range  $Z$

between 15 and 25 mm. This shows that the inner recirculation zone (IRZ) attracts droplets that are diverted from the fresh gas cone.

In reactive conditions, the droplet dynamics are highly influenced by the flame that is stabilized very close to the chamber entrance. For high staging factors, OP<sub>60</sub> in Fig. 5, the pilot stage stabilizes the flame and the stabilization point is located inside the injection device, leading to high radial velocities  $\bar{V}_z$ . When the flame is stabilised by the multi-injection stage (OP<sub>20</sub>), there is a slight shift of the axial velocity  $\bar{V}_x$  profile towards the IRZ, which can be related to the transition from the V-shape to the M-shape. This means that the fresh gas cone angle changes. Radial velocities  $\bar{V}_z$  become very low. Finally the OP<sub>35</sub> case (intermediate stabilization) has a similar behavior as the OP<sub>60</sub> one in its inner structure and a similar behavior as OP<sub>20</sub> for its outer part. The cone angle deduced from Fig. 5(a) is in-between. In these reactive situations, no negative values of  $\bar{V}_z$  are visible, meaning that the droplets are burnt before being diverted from the fresh gas penetration cone.

### Sauter mean diameter

The Sauter mean diameter (SMD) profile is shown in Figs. 4(c) and 5(c) respectively for the non-reactive and reactive cases. In the core of the penetration cone, the droplet diameter is lower than in its periphery. This may be due to the higher velocities encountered by the droplets inside the cone, which may cause a better atomization and a faster vaporization. Globally, results show a slight effect of the staging factor  $\alpha$  as SMDs increase with this parameter. To illustrate this point, Fig. 6 shows the droplet diameter distribution for the three values of the staging factor, at  $X = 15$  mm and  $Z = 28$  mm. Increasing  $\alpha$  results in a slight increase of the number of higher diameter droplets, explaining the difference in SMDs in the core of the spray. The same phenomenon is observed in droplet diameter distribution for the reactive cases.

### Unsteady flow dynamics

From the randomly sampled data acquired by the PDA system, all the signals were re-sampled at 16 kHz and 6 kHz for the non-reactive and reactive flow respectively. Figure 7 shows an example of the re-sampled radial velocity component  $V_z^*$  at  $X = 15$  mm,  $Y = 0$  mm and  $Z = 26$  mm, and for OP<sub>60</sub>.

**Non-reactive flow dynamics** Using the re-sampled signals, a spectral analysis is carried out on the non-reactive flow. Figure 8 shows the Power Spectral Density (PSD) of the re-sampled diameter and radial velocity signals at  $Z = 26$  mm for OP<sub>60</sub>. The PSD was computed using the Welch method, with fifty periodograms, a hundred blocks, Hanning window and a spectral resolution of 16 Hz.

Both spectra show a peak at the same frequency

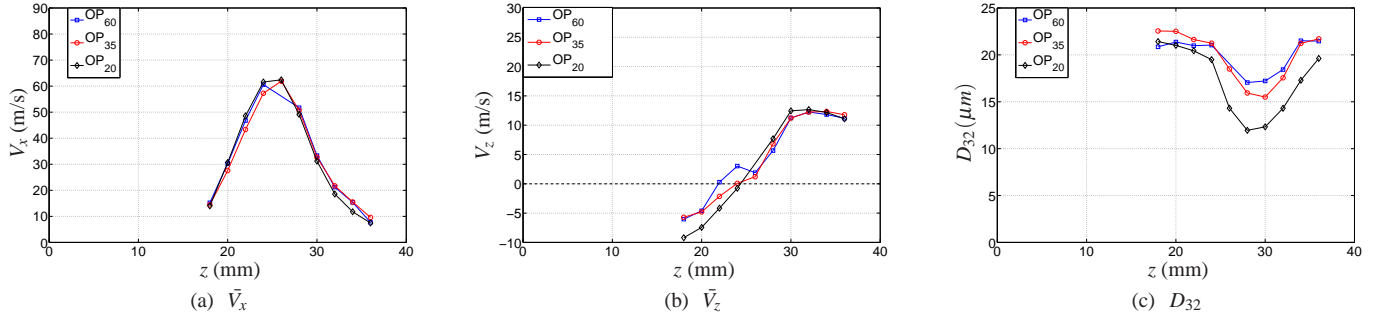


**FIGURE 4.** NON-REACTIVE FLOW. AXIAL VELOCITY  $\bar{V}_x$ , RADIAL VELOCITY  $\bar{V}_z$  AND SAUTER MEAN DIAMETER  $D_{32}$  PROFILES AT  $X = 15$  MM AND  $Y = 0$  MM.

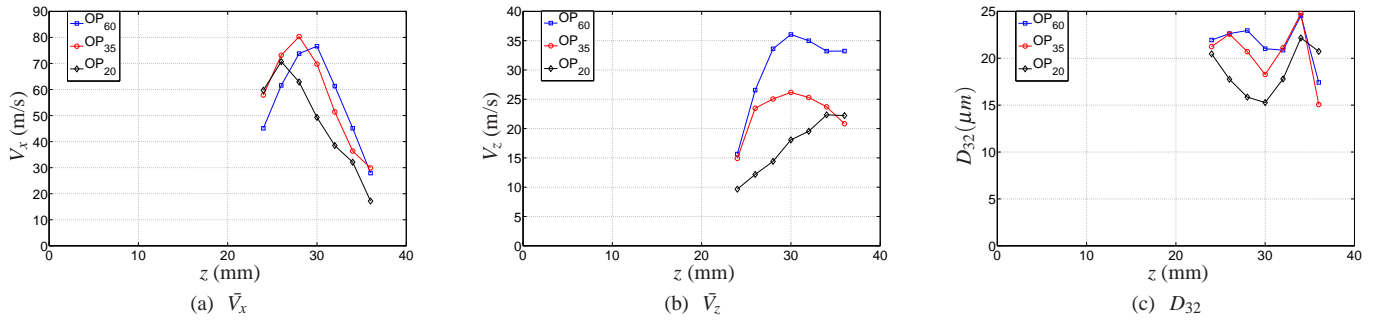


**FIGURE 5.** REACTIVE FLOW. AXIAL VELOCITY  $\bar{V}_x$ , RADIAL VELOCITY  $\bar{V}_z$  AND SAUTER MEAN DIAMETER  $D_{32}$  PROFILES AT  $X = 15$  MM AND  $Y = 0$  MM.

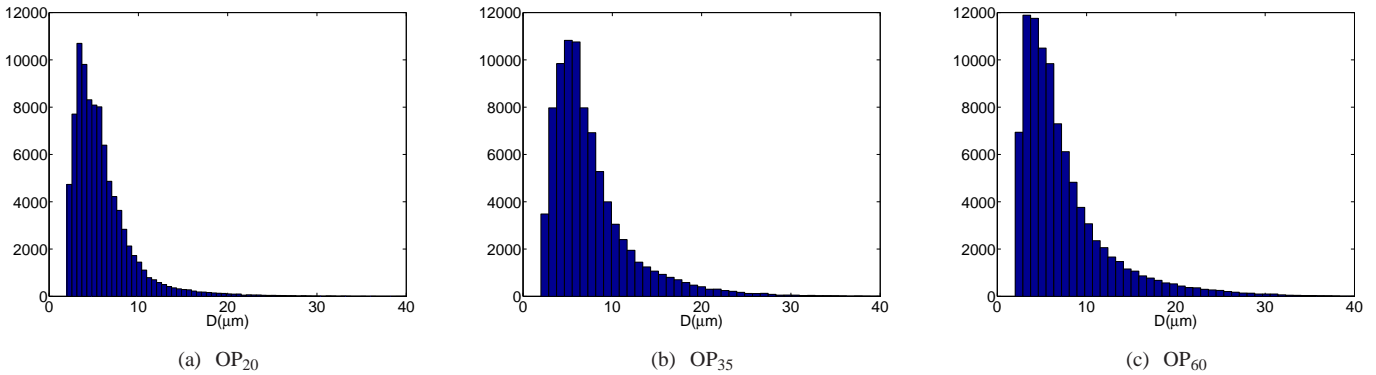


**FIGURE 6.** NON-REACTIVE FLOW. DROPLET DIAMETER DISTRIBUTION FOR THE DIFFERENT VALUES OF THE STAGING FACTOR.  $X = 15$  MM AND  $Z = 28$  MM.

$f_F^{NR} = 2500$  Hz, visible at all the staging values even if a decrease in the peak amplitude is observed for lower  $\alpha$ . Recent work on the same configuration [22] has shown that this frequency peak is associated with a three-dimensional structure, such as the Precessing Vortex Core (PVC), often encountered in swirling flows [23]. Numerical simulations on a similar geometry revealed the presence of a PVC, taking initially place near the pilot stage [24]. This may explain why reducing  $\alpha$  (i.e.

less fuel is injected through the pilot stage) can cause a decrease in the rotating structure visualization.

Using the mean arithmetic diameter, computed in regions where the spectral analysis is performed, and the characteristic frequency of the flow  $f_F^{NR}$ , it is possible to estimate a Stokes number  $\bar{S}t$  for the droplets submitted to the perturbation. Computing the mean Stokes number in regions where the

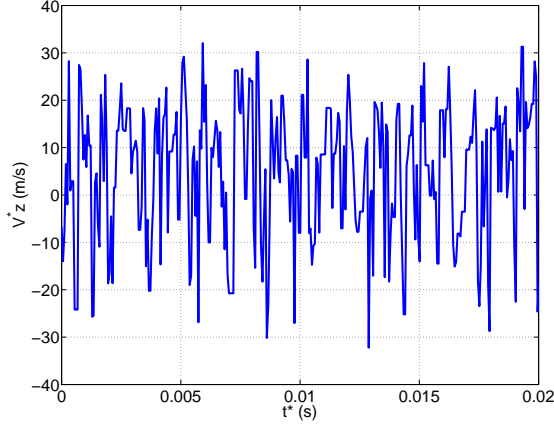


**FIGURE 7.** NON-REACTIVE FLOW. EXAMPLE OF THE RE-SAMPLED RADIAL VELOCITY  $V_z^*$  AT  $X = 15$  MM,  $Y = 0$  MM,  $Z = 26$  MM AND FOR OP<sub>60</sub>.

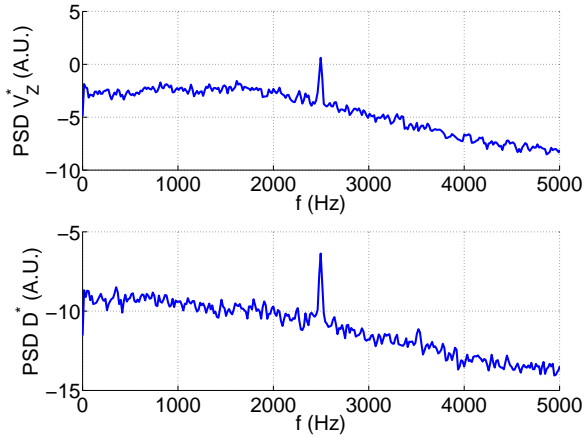


**FIGURE 8.** NON-REACTIVE FLOW. PSD OF THE RE-SAMPLED RADIAL VELOCITY  $V_z^*$  (TOP) AND DIAMETER  $D^*$  (BOTTOM) AT  $Z = 26$  MM AND FOR OP<sub>60</sub>.

spectral content is high at  $f_F^{NR}$  gives  $\bar{St} \approx 0.1$ , which is quite low. This suggests that the droplets in this region may be small enough to follow the gaseous flow, which is mainly imposed by the air. As a consequence, changing the staging factor has little influence on the non-reactive droplet velocity distribution, piloted by the strong rotating coherent structure.

Taking the re-sampled radial velocity  $V_z^*$  as a reference signal, a phase-lock averaging method is introduced to estimate the mean behavior of droplets at  $X = 15$  mm. In two-phase flows, carrying out a phase-lock averaging method is only possible in

regions where droplets are small enough to be considered as describing the gaseous phase. Therefore, this averaging method is only applied in regions where the Stokes number was estimated and found small enough to validate the procedure. The phase-locked mean cycle was decomposed in 20 phases, every  $18^\circ \pm 9^\circ$  using approximately 2,000 instantaneous values for each phase. Figure 9 shows the fluctuations of the phase averaged axial and radial velocities and diameter, respectively  $V_{x\Phi}^*$ ,  $V_{z\Phi}^*$  and  $D_\Phi^*$ .

Both velocity components show a strong oscillation at the flow frequency  $f_F^{NR}$ . Fluctuations are particularly high for the radial component  $V_{z\Phi}^*$ , which is certainly due to the fact that this frequency is associated with a precessing rotating structure. Still,  $V_{x\Phi}^*$  also shows a non-negligible fluctuation at the same frequency (Fig. 9(a)). More surprisingly, the phase averaged diameter signal shows a coherent oscillation of about 5 to 10% of the mean arithmetic diameter, which is more or less synchronized with the velocity fluctuations. Further investigations are needed on this last point. Traveling along the  $Z$  axis, similar results are found, with a clear oscillation of  $V_{x\Phi}^*$ ,  $V_{z\Phi}^*$  and  $D_\Phi^*$ .

In a recent work on the non-reactive flow, the Mie intensity fluctuations of the spray were measured in transverse plans using synchronized high speed laser and camera [22]. Spectral analysis was carried out in the laser plan, and the same frequency peak was retrieved. With this diagnostic setup, it was possible to show that two points on opposite sides of the spray diameter presented Mie intensity fluctuations with a phase shift of  $180^\circ$ . Relating the Mie scattering intensity to the droplet density, one can imagine that the rotating hydrodynamic structure (PVC) strongly impact both the density and droplet diameter distributions in these regions.

**Reactive flow dynamics** For this second part of the spectral analysis, two regions of interest A and B are defined, corresponding respectively to  $Z = 32$  mm and  $Z = 30$  mm, as shown in Fig. 3. These regions present acquisition data rates high enough for the analysis. Raw signals from the PDA were re-sampled at 6 kHz and a PSD was computed in both regions, using the Welch method, with approximately 30 periodograms, 59 blocks, Hanning window and a spectral resolution of 4 Hz. Figures 10 and 11 successively show the PSD of the heat release rate (OH\* chemiluminescence), acoustic pressure and radial velocity re-sampled signals.

The acoustic pressure signal reveals a strong peak centered at  $f_{ac} = 280$  Hz, which is also seen by the OH\* spontaneous emission signal, both in phase, as expected by the Rayleigh criterion in case of thermo-acoustic instabilities. As expected, the re-sampled radial velocity  $V_z^*$  shows in region A a strong peak at  $f_{ac}$  as well, indicating that the instability strongly modifies the spray dynamics (Fig. 11, top). More interestingly, a small peak at  $f_F^R = 2620$  Hz is visible in the second part of the spectrum. In

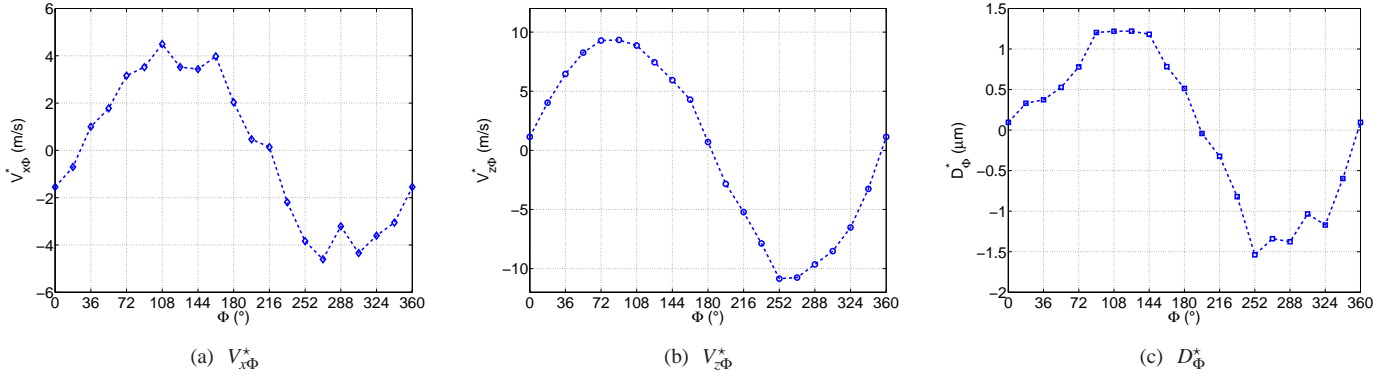


**FIGURE 9.** NON-REACTIVE FLOW. FLUCTUATIONS OF THE PHASE AVERAGED AXIAL VELOCITY  $V_{x\Phi}^*$ , RADIAL VELOCITY  $V_{z\Phi}^*$  AND DIAMETER  $D_{\Phi}^*$  AT  $F_f^{NR} = 2500$  Hz AND FOR  $OP_{60}$ .  $X = 15$  MM,  $Y = 0$  MM AND  $Z = 26$  MM.

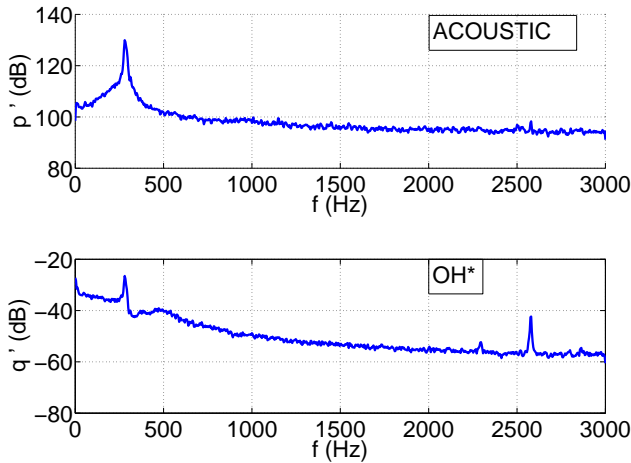


**FIGURE 10.** PSD OF ACOUSTIC PRESSURE AND HEAT RELEASE RATE, REGION A,  $OP_{60}$ .

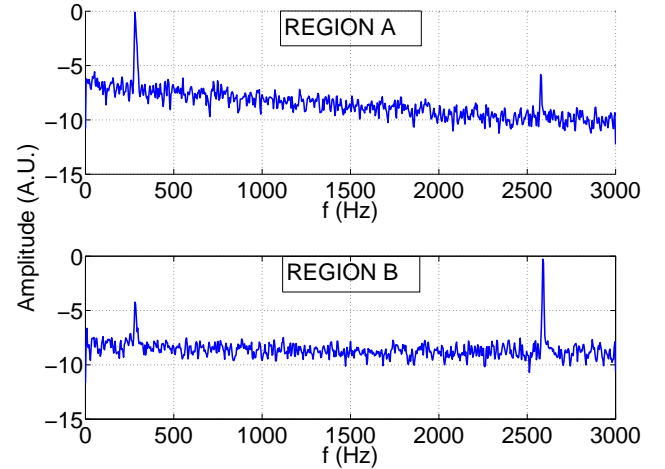


**FIGURE 11.** PSD OF THE RE-SAMPLED RADIAL VELOCITY  $V_z^*$ , REGION A AND B,  $OP_{60}$ .

region B, this high frequency peak becomes even preponderant, compared to the thermo-acoustic low frequency peak (Fig. 11, bottom). Both peaks are also visible on the resampled axial velocity  $V_x^*$  and diameter  $D^*$  signals. One would wish to associate  $f_F^R$  to the rotating structure highlighted in the non-reactive situation ( $F_f^{NR} = 2500$  Hz); the frequency increase would be due to the flow acceleration due to the combustion process. Still, other possibilities exist and one must remain careful. Complementary investigations will be carried out.

Still, the acoustic pressure and the heat release rate signals hardly show the high frequency peak, and one can imagine that this is due to the fact that this is a pure hydrodynamic motion, uncorrelated with the thermo-acoustic oscillation [25]. Moreover, it is shown in [26] that the thermo-acoustic frequency peak is dom-

inant in the jet region while the PVC frequency peak is higher in the inner shear layer (ISL). Looking closely at regions A and B seems to confirm this last point, as region B can be considered as belonging to the ISL, while region A would belong to the penetrating conical jet region.

The spectral analysis was carried out for the three values of  $\alpha$ . No change was observed on the high frequency peak, partially confirming its hydrodynamic nature. In the same time, the thermo-acoustic frequency peak is slightly shifted. At low  $\alpha$ , the thermo-acoustic peak emerges with a frequency around 300 Hz and for in-between values, the peak was detected at 252 Hz.

These results show that the phase-lock averaging method

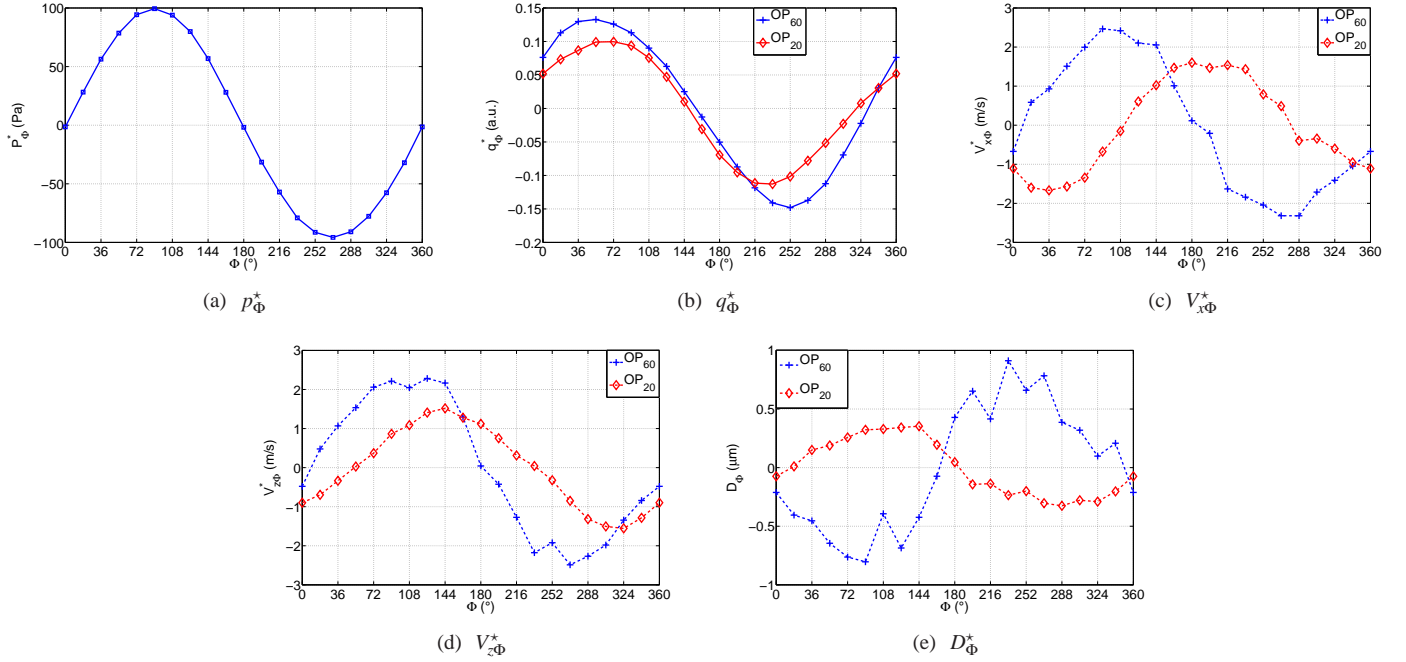


**FIGURE 12.** FLUCTUATIONS OF THE PHASE AVERAGED ACOUSTIC PRESSURE  $p_{\Phi}^*$ , HEAT RELEASE RATE  $q_{\Phi}^*$ , DIAMETER  $D_{\Phi}^*$ , AXIAL VELOCITY  $V_{x\Phi}^*$  AND RADIAL VELOCITY  $V_{z\Phi}^*$ . REGION A,  $f_{ac} = 280$  Hz, OP<sub>60</sub> and  $f_{ac} = 300$  Hz, OP<sub>20</sub>.

can be performed in the regions where the thermo-acoustic instability is predominant, at the lower frequencies  $f_{ac} = 280$  Hz and  $f_{ac} = 300$  Hz for OP<sub>60</sub> and OP<sub>20</sub> respectively. For OP<sub>35</sub>, even though thermo-acoustic activity emerges in the range [250-300] Hz in the pressure fluctuations, with a peak at 252 Hz, no peak at this particular frequency could be observed on the droplet diameter signal. On the contrary, the peak at 256 Hz is still present. The absence of a peak in the diameter at the combustion instability frequency may be the result of its relatively lower amplitude (108 dB).

The post-processing is carried out in region A to analyze the influence of the thermo-acoustic instability on the droplet's behavior, by taking the pressure signal as the time reference signal [27]. In region B, where the hydrodynamic instability is the dominant phenomenon, it is not possible to apply the phase-lock averaging technique to the dominant instability. Recent work on this subject [26] shows that, even when the acoustic coupling occurs with a much lower amplitude compared to the hydrodynamic phenomenon, it is not possible to describe the flow behavior at the higher frequency and neglect the lower one. In this last case, a two-phase-lock averaging method needs to be developed. This work is still in progress.

The average cycle is divided into 20 phases, every  $18^{\circ} \pm 9^{\circ}$  using approximately 2,000 instantaneous values for each phase. Figure 12 shows the average cycle for the acoustic pressure, heat release rate, axial and radial velocities, and diameter. Results

indicate that droplet's velocity components are almost in phase with the pressure fluctuations for OP<sub>60</sub> while OP<sub>20</sub> shows a shift for both velocities. The impact on the diameter is visible, as in the high frequency oscillation observed in the non-reactive case, but for the OP<sub>60</sub>, the diameter evolution is out of phase, compared to the pressure and droplet velocity signals. This shows that the thermo-acoustic instability and the staging factor strongly influence the spray behavior.

Studies on droplet and spray behavior submitted to acoustic fields have shown that acoustic and convective fluctuations can be present, leading to different droplet responses, in term of amplitude and phase [28, 29, 30, 31]. The driving process can depend on various parameters: spray distribution in terms of size and velocity, frequency and amplitude of fluctuations, etc., and it is crucial to investigate the type of interaction that occurs in the system.

The first idea can be to reconstruct the local acoustic velocity by applying the Hilbert transform on the pressure time-signal from microphones M2 and M3 as defined below [32]:

$$u_{ac}(x, t) = \text{Re} \left( \frac{\mathcal{H}(p(M3)) - \mathcal{H}(p(M2))}{\rho_a \omega \Delta x} \right) \quad (4)$$

where Re is the real part of a complex quantity and  $\Delta x = 0.18$  m

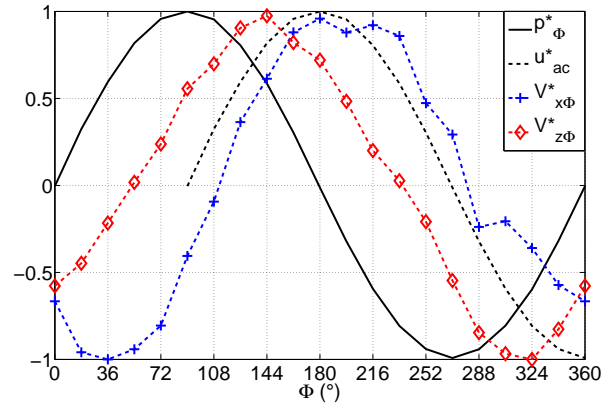
corresponds to the spacing between the two microphones. This reconstruction is only possible when the spacing between the two microphones is much smaller than the acoustic wavelength. In the present case, the wavelength has been estimated close to  $\lambda_{ac} = 2.5$  m, leading to  $\lambda_{ac}/\Delta x = 14$ .

This reconstruction gives a good estimate of the acoustic velocity in the combustion chamber. For both operating conditions, it was found that the acoustic velocity presented a phase delay of  $90^\circ$  compared to the acoustic pressure. Figure 13 shows the average cycle for the relative fluctuations of the two velocity components and acoustic pressure and velocity for OP<sub>20</sub> and OP<sub>60</sub>. Several studies on the interaction of a spray with an acoustic field [33, 34, 35] have shown that when located at an acoustic velocity antinode, the spray velocity field decreases in magnitude, accompanied with a decrease in droplet size. The results obtained in the OP<sub>20</sub> case are consistent with this conclusion. The axial velocity presents a slight phase shift with the acoustic velocity and diameters show negative fluctuations (Fig. 12(e)). When the droplet's motion is influenced by the acoustic field, then the phase shift of the droplet axial velocity will essentially depend on its size [29, 33, 34]. This means in particular that a more precise study looking at the phase shift as a function of droplet distribution should be undertaken.

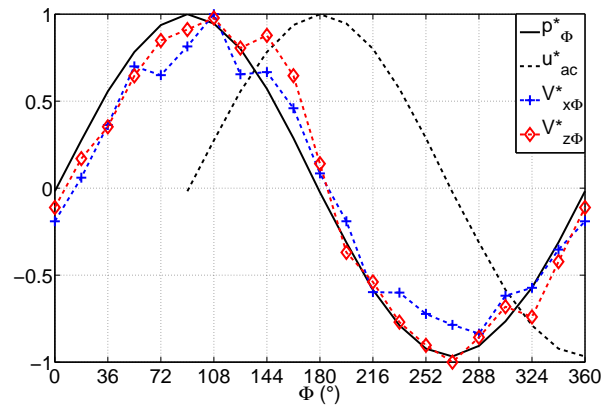
This does not explain the spray behavior observed in the OP<sub>60</sub> case. Moreover, trying to estimate the acoustic velocity amplitude using the simplistic relation  $u'_{ac} \approx p'/\rho a c$ , which is only valid for plane wave progressive propagation, one finds  $u'_{ac} \approx 0.4$  m · s<sup>-1</sup>. Droplets show here velocity fluctuations 3 or 4 times higher (cf. Fig. 12). One suggestion could be that the acoustic field modulates the flow and the nascent spray inside the injector, resulting in large coherent structures that are generated at the acoustic frequency and convected by the flow [28, 30, 31, 36]. In addition, table 1 shows that the liquid pressure loss is much larger in the pilot stage compared to the takeoff stage. In this last case, where the drop is of the order of 100 mbar, one can imagine a very strong influence of the acoustic waves on the spray's dynamical response.

Droplets trapped in these coherent structures would present velocity fluctuations much higher than the acoustic ones. By taking the mean velocity of a droplet in reactive conditions in region A ( $V_x \approx 75$  m · s<sup>-1</sup>), one can estimate the convective delay between the injector exit and the measurement location ( $X = 15$  mm). This approach results in a  $22^\circ$  phase delay, which seems consistent with the experimental results.

In conclusion, while results for OP<sub>20</sub> are consistent with several studies on interaction of sprays with strong acoustic fields, OP<sub>60</sub> shows a completely different response of the spray. The change in the droplet's motion may be explained by two main differences between the two operating conditions:



(a)  $f_{ac} = 300$  Hz, OP<sub>20</sub>



(b)  $f_{ac} = 280$  Hz, OP<sub>60</sub>

**FIGURE 13.** RELATIVE FLUCTUATIONS OF THE PHASE AVERAGED ACOUSTIC PRESSURE  $p^*_{\Phi}$ , ACOUSTIC VELOCITY  $u^*_{ac}$ , AXIAL VELOCITY  $V^*_{x\Phi}$  AND RADIAL VELOCITY  $V^*_{z\Phi}$ , NORMALIZED BY ITS RESPECTIVE MAXIMUM. REGION A.

1. **flame stabilization:** OP<sub>60</sub> results in a V-flame stabilized inside the injection device while for OP<sub>20</sub> the flame is completely stabilized in the combustion chamber. The different stabilization process and position of the flame may affect the global acoustics of the system. Furthermore, for OP<sub>20</sub>, droplet velocities are measured close to the flame base whereas for OP<sub>60</sub>, velocities are acquired downstream the flame's stabilization point (OP<sub>60</sub>). In the later case, this may suggest that droplets are influenced by two different acoustic fields.
2. **fuel distribution:** while the majority of the fuel is injected through the takeoff stage for OP<sub>20</sub>, OP<sub>60</sub> generates a global spray, where droplets motion may highly differ whether is a droplet created at the takeoff or the pilot stage. In addition, the droplet diameter distribution for the two operating conditions are presented in Fig. 14 and it is seen that distributions

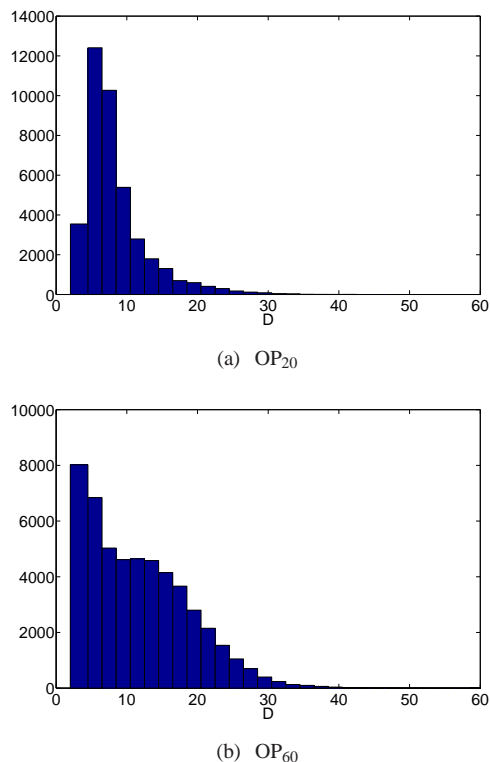


**FIGURE 14.** DROPLET DIAMETER DISTRIBUTION FOR OP<sub>20</sub> and OP<sub>60</sub>- REGION A.

are highly different.

Of course, other explanations may be envisaged, and further investigations are carried out on this issue.

## CONCLUSION

A laboratory-scale staged multi-injection combustor is described in the present paper, in the framework of LPP combustion. Using a staging procedure between the primary pilot stage and the secondary multipoint one, droplet and velocity field distributions can be varied in the spray that is formed at the entrance of the combustion chamber. In the reactive case, three different stabilization processes occur, depending on the staging factor. Three staging values, corresponding to these three different flame stabilization processes, are analyzed both in non-reactive and reactive situations, while power is kept constant. Non-reactive and reactive flows are characterized through an extensive Phase Doppler Anemometry (PDA) campaign. Data are acquired along two directions of the chamber.

It is first shown that mean values and droplet distributions can be affected by the staging value in the non-reactive as in the reactive situations. Using adequate post-processing, it is

also possible to study non-reactive and reactive flow/flame dynamics. Spectral analysis shows that the non-reactive flow is strongly structured by a high frequency rotating structure that can clearly be associated with a precessing vortex core (PVC). In this situation,  $f_F^{NR} = 2500$  Hz. The structure frequency is not modified while changing the staging factor. A phase-lock averaging method shows that velocity components and droplet distributions are in phase.

The reactive situation encounters a strong acoustic-flame coupling leading to a low frequency oscillation of both the velocity field and the spray droplet distribution at  $f_{ac} = 280$  Hz and  $f_{ac} = 300$  Hz depending on the fuel distribution. In this situation, high frequency phenomena, which may be due to PVC, are still visible, with a second peak frequency  $f_F^R = 2620$  Hz, which can become predominant in some regions. In the regions where the thermo-acoustic instability is the strongest phenomenon, the same phase averaging procedure can be applied. On one hand, for OP<sub>60</sub>, pressure, heat release and velocity are in phase while the diameter signal seems out of phase. Further investigations are necessary on this last point. On the other hand, OP<sub>20</sub> results are consistent with several studies on the interaction of a spray with a strong acoustic field. The different behavior observed for each operating conditions may come from the different mechanisms of flame stabilization and the interaction of droplets coming simultaneously from the two stages (OP<sub>60</sub>).

## ACKNOWLEDGMENTS

This work is supported by Pôle ASTECH and funded by Conseil Régional d'Ile-de-France (CRIF), in the framework of the INCA initiative. The authors would like to thank the technical staff at the EM2C laboratory for their help in designing and mounting the experimental setup.

## REFERENCES

- [1] Correa, S., 1998. "Power generation and aeropropulsion gas turbines: From combustion science to combustion technology". *Proceedings of the Combustion Institute*, **27**, pp. 1793–1807.
- [2] Tacina, R., 1990. "Low nox potential of gas turbine engines". *AIAA Aerospace Sciences Meeting and Exhibit(90-0550)*, January.
- [3] Lefebvre, A., 1995. "The role of fuel preparation in low-emission combustion". *Journal of Engineering for Gas Turbines and Power*, **117**, pp. 617–654.
- [4] Moore, M., 1997. "Nox emission control in gas turbines for combined cycles cycle gas turbine plant". *Journal of Power and Energy*, **211**(1), pp. 43–52.
- [5] Lieuwen, T., and Yang, V., 2006. *Combustion Instabilities in Gas Turbine Engines: Operational Experience, Funda-*

- mental Mechanisms, and Modeling*, Vol. 210. Progress in Astronautics and Aeronautics.
- [6] Candel, S., 2002. “Combustion dynamics and control progress and challenges”. *Proceedings of the Combustion Institute*, **29**, pp. 1–28.
- [7] Nauert, A., Petersson, P., Linne, M., and Dreizler, A., 2007. “Experimental analysis of flashback in lean premixed swirling flames: conditions close to flashback”. *Experiments in Fluids*, **43**, pp. 89–100.
- [8] Lefebvre, A., 1999. *Gas Turbine Combustion*, 2nd ed. Taylor & Francis.
- [9] Ducruix, S., Schuller, T., Durox, D., and Candel, S., 2003. “Combustion dynamics and instabilities: elementary coupling and driving mechanisms”. *Journal of Propulsion and Power*, **19**(5), Sep-Oct, pp. 722–734.
- [10] Neumeier, Y., and Zinn, B. T., 1996. “Experimental demonstration of active control of combustion instabilities using real-time modes observation and secondary fuel injection”. *Symposium (International) on Combustion*, **26**(2), pp. 2811–2818.
- [11] Lee, J., Kim, K., and Santavicca, D., 2000. “Effect of injection location on the effectiveness of an active control system using secondary fuel injection”. *Proceedings of the Combustion Institute*, **28**, pp. 739–746.
- [12] Bernier, D., Ducruix, S., Lacas, F., Candel, S., Robart, N., and Poinot, T., 2003. “Transfer function measurements in a model combustor: Application to adaptive instability control”. *Combustion Science and Technology*, **175**, pp. 993–1013.
- [13] Tachibana, S., Zimmer, L., Kurosawa, Y., and Suzuki, K., 2007. “Active control of combustion oscillations in a lean premixed combustor by secondary fuel injection coupling with chemiluminescence imaging technique”. *Proceedings of the Combustion Institute*, **31**(2), pp. 3225–3233.
- [14] Barbosa, S., de La Cruz Garcia, M., Ducruix, S., Labégorre, B., and Lacas, F., 2007. “Control of combustion instabilities by local injection of hydrogen”. *Proceedings of the Combustion Institute*, **31**(2), pp. 3207–3214.
- [15] Sjöblom, B., and Rehn, J., 1997. “The volvo high-speed generation hybrid drive and associated combustion system”. *Energy Conversion and Management*, **38**(10-13), pp. 1225–1235.
- [16] Barbosa, S., Scoufflaire, P., and Ducruix, S., 2009. “Time resolved flowfield, flame structure and acoustic characterization of a staged multi-injection burner”. *Proceedings of the Combustion Institute*, **32**(2), pp. 2965 – 2972.
- [17] Batarseh, F., Gnirß, M., Roisman, I., and Tropea, C., 2009. “Fluctuations of a spray generated by an airblast atomizer”. *Experiments in Fluids*, **46**(6), pp. 1081–1091.
- [18] Galley, D., Ducruix, S., Lacas, F., and Veynante, D., 2011. “Mixing and stabilization study of a partially premixed swirling flame using laser induced fluorescence”. *Combustion and Flame*, **158**, pp. 155–171.
- [19] Hardalupas, Y., and Taylor, A., 1989. “On the measurement of particle concentration near a stagnation point”. *Experiments in Fluids*, **8**, pp. 113–118. 10.1007/BF00203075.
- [20] Cossali, E., and Hardalupas, Y., 1992. “Comparison between laser diffraction and phase doppler velocimeter techniques in high turbidity, small diameter sprays”. *Experiments in Fluids*, **13**, pp. 414–422. 10.1007/BF00223249.
- [21] Gupta, A., Lilley, D., and Syred, N., 1984. *Swirl Flows*. Energy and Engineering Science Series.
- [22] Providakis, T., Scoufflaire, P., Zimmer, L., and Ducruix, S., 2010. “Time-resolved piv measurements applied to a non-reactive dodecane-air mixture in a two-staged multi-injection burner”. *15th Int Symp on Applications of Laser Techniques to Fluid Mechanics*, July.
- [23] Syred, N., 2006. “A review of oscillation mechanisms and the role of the precessing vortex core (pvc) in swirl combustion systems”. *Progress in Energy and Combustion Science*, **32**, pp. 93–161.
- [24] Jaegle, F., Senoner, J.-M., Garcàa, M., Bismes, F., Lecourt, R., Cuenot, B., and Poinot, T., 2011. “Eulerian and lagrangian spray simulations of an aeronautical multipoint injector”. *Proceedings of the Combustion Institute*, **33**(2), pp. 2099 – 2107.
- [25] Boxx, I., Stöhr, M., Carter, C., and Meier, W., 2010. “Temporally resolved planar measurements of transient phenomena in a partially pre-mixed swirl flame in a gas turbine model combustor”. *Combustion and Flame*, **157**(8), pp. 1510 – 1525.
- [26] Steinberg, A. M., Boxx, I., Stöhr, M., Carter, C. D., and Meier, W., 2010. “Flow-flame interactions causing acoustically coupled heat release fluctuations in a thermoacoustically unstable gas turbine model combustor”. *Combustion and Flame*, **157**(12), 12, pp. 2250–2266.
- [27] De la Cruz Garcia, M., Mastorakos, E., and Dowling, A., 2009. “Investigations on the self-excited oscillations in a kerosene spray flame”. *Combustion and Flame*, **156**, pp. 374–384.
- [28] Haile, E., Delabroy, O., Lacas, F., Veynante, D., and Candel, S., 1996. “Structure of an acoustically forced turbulent spray flame”. In *Twenty-Sixth Symposium (International) on Combustion*, The Combustion Institute, pp. 1663–1670.
- [29] Sujith, R. I., 2003. “An experimental investigation of jets in a strong acoustic field”. *AIAA*(2003-1276).
- [30] Gajan, P., Strzelecki, B., Platet, B., Lecourt, R., and Giuliani, F., 2007. “Investigation of spray behavior downstream of an aeroengine injector with acoustic excitation”. *Journal of Propulsion and Power*, **23**(2), March-April, pp. 390–397.
- [31] Lacour, C., Durox, D., Ducruix, S., and Massot, M., 2011. “Interaction of a polydisperse spray with vortices”. *Experiments in Fluids*. DOI: 10.1007/s00348-011-1050-1.

- [32] Tran, N., 2009. “Influence de la condition limite acoustique amont sur les instabilités de combustion de grande amplitude: Conception d’un système robuste de contrôle d’impédance”. PhD thesis, Ecole Centrale Paris.
- [33] Sujith, R. I., Waldherr, G. A., Jagoda, J. I., and Zinn, B., 1997. “An experimental investigation of the behavior of droplets in axial acoustic fields”. *Journal of Vibration and Acoustics*, **119**, pp. 285–292.
- [34] Sujith, R. I., 2005. “An experimental investigation of interaction of sprays with acoustic fields”. *Experiments in Fluids*, **38**, pp. 576–587. 10.1007/s00348-004-0912-1.
- [35] Eckstein, J., Freitag, E., Hirsch, C., Sattelmayer, T., Von der Bank, R., and Schilling, T., 2005. “Forced low-frequency spray characteristics of a generic airblast swirl diffusion burner”. *Journal of Engineering for Gas Turbines and Power*, **127**(301).
- [36] Birbaud, A. L., Durox, D., Ducruix, S., and Candel, S., 2007. “Dynamics of free jets submitted to upstream acoustic modulations”. *Physics of Fluids*, **19**(1), p. 013602.